ANISOTROPY OF MAGNETIC SUSCEPTIBILITY ANALYSIS OF THE RUSCA-TIHU VOLCANICLASTIC FORMATION (EAST CARPATHIANS): FLOW DIRECTIONS RECOGNITION

S.A. ŞORTAN[1], C.G. PANAIOTU[2*], D. DIMOFTE[1], R.D. ROBAN[1], C. NECULA[2]

[1] University of Bucharest, Faculty of Geology and Geophysics, Bucharest, Romania
E-mails: *sonia3sortan@gmail.com, danidimofte@gmail.com, reludumitru.roban@g.unibuc.ro*
[2] University of Bucharest, Faculty of Physics, Bucharest-Măgurele, Romania
E-mails: *cristian.panaiotu@g.unibuc.ro, c3necula@yahoo.com*
[*]Corresponding author: *cristian.panaiotu@g.unibuc.ro*

Abstract. This anisotropy of magnetic susceptibility and rockmagnetic study reveals several features about the Upper Miocene pyroclastic deposits of the Călimani Mountains. The general trend of inferred flow directions toward south is compatible with the supposed position of eruption centers. The emplacement temperature of the studied pyroclastic deposits was below 300°C.

Key words: anisotropy of magnetic susceptibility, pyroclastic deposits, East Carpathians.

1. INTRODUCTION

Paleomagnetic and rock magnetic techniques have been widely applied to solve various problems in volcanology [1]. In the past decades the anisotropy of magnetic susceptibility (AMS) was used to evaluate flow directions in pyroclastic flow deposits to determine the source vent locations, since former volcanic centers may be either eroded or covered by younger deposits. The AMS reflects the preferred orientation and the shape of minerals in rocks *i.e.* its magnetic fabric [2]. As petrological structures (*e.g.* foliation or lineation) are often difficult to observe and measure in volcaniclastic rocks, the AMS may be the only way to find reliable transport directions in these rocks [3].

The main objective of the present study is to determinate flow directions using the AMS in one of the largest pyroclastic deposits in Romania: the Rusca-Tihu Volcaniclastic Formation from the Călimani Mountains (East Carpathians). Previous AMS analysis have determined the flows directions in lavas from the southern part of the Călimani-Gurghiu-Harghita volcanic chain [4], so this study is the first attempt to obtain AMS data from pyroclastic rocks to infer the flow directions.

2. GEOLOGICAL SETTING AND METHOD

During the last 15 Ma, westward-dipping subduction caused the collision of two lithospheric blocks from the west with the south-eastern border of the European Platform [5]. Volcanism started to take place in the Călimani–Gurghiu–Harghita volcanic chain (East Carpathians) around 11 Ma in the Călimani Mountains. The magmatic history of the Călimani Mountains involves eruptions that occurred between 11.3–6.7 Ma [6]. Rusca-Tihu Volcano is one of the largest identifiable strato-volcanoes in these mountains with a wide range of volcaniclastic products generated, from lava flows and lava domes to pyroclastic flows and block-and-ash flow deposits of basic andesite or basaltic andesite composition [7]. It was also shown in several papers [7, 8] that the tectonic instability was the most likely cause of the edifice failure around 8.0 ± 0.5 Ma, which resulted into a debris avalanche that reached distances of tens of km. The deposits of post-debris-avalanche volcanic activity have been denominated as the Rusca-Tihu Volcaniclastic Formation (RTF in Fig. 1) [7]. These deposits were formed around 8 – 7.5 Ma [7].

The samples were collected from sites located in quarries and road cuts in the Răstolița Dam area (Fig 1 and Table 1): 6 sites in fine poorly lithified phreatomagmatic deposits and 2 sites in the inter-bedded lava flows. Sampling was done with a water cooled portable electric drill in soft pyroclastic deposits and a petrol-powered portable drill in lava flows. All samples were oriented in situ both with a magnetic compass and a solar compass. The thickness of the sampled deposits is around 1–2 m. All sampled strata are horizontal.

The measurements were carried out in the Paleomagnetic Laboratory of the University of Bucharest. In addition to the magnetic measurements, we have analyzed the mineralogy of sampled sites using thin sections. From each sample standard cylindrical specimens were cut (2.5×2.2 cm). We have used the same protocols as in [4, 9] to identify the magnetic properties of the studied rocks. Field dependence of magnetic susceptibility was measured with the MFK1-A Kappabridge (AGICO) in two fields: 50 A/m and 700 A/m. The variation of magnetic susceptibility with temperature was measured in argon atmosphere with a CS-3 furnace coupled with the MFK1-A Kappabridge; the heating-cooling cycle measurements were done from room temperature to 700°C. The magnetic domain state of the ferromagnetic minerals was determined using hysteresis parameters measured with a Micromag VSM model 3900: remanent saturation magnetization (M_{rs}), saturation magnetization (M_s), coercivity of remanence (H_{cr}) or coercivity (H_c). The FORC (First Order Reversal Curves) measurements were made using the irregular FORC protocol of [10]. Isothermal remanent magnetizations (IRM) were imparted using a pulse magnetizer in a direct field of 1 T and backfield of 0.3 T and measured with a JR6A magnetometer (AGICO).

The AMS measurements were carried out using a 3D rotator coupled with the MFK1-A Kappabridge. AMS data were analyzed using Anisoft 5.1.01 (AGICO).

The structure of the natural remanent magnetization was determined using both AF (alternating field) demagnetization and thermal demagnetization and the equipment presented in [11]. All remanences were measured with a JR6A magnetometer and analyzed using Remasoft 3.0 (AGICO).
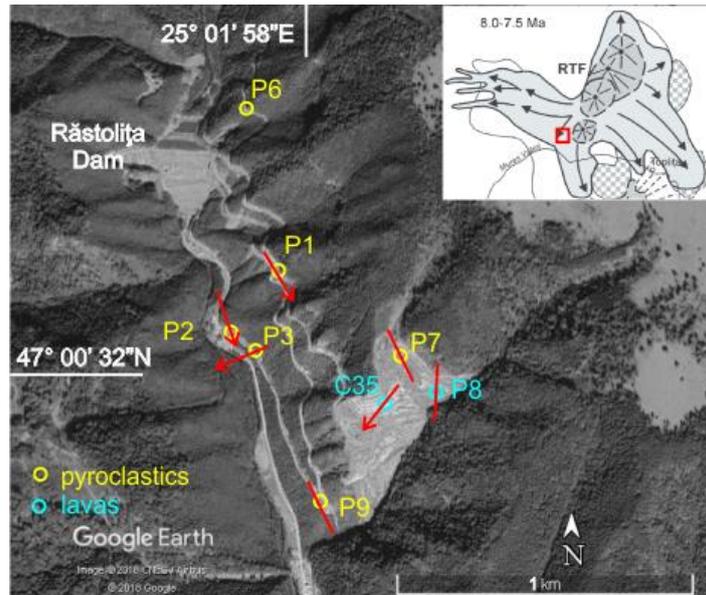

Fig. 1 – (Color online). Location of the sampling sites. The inlet shows the position of the sampling area (red rectangle) within the Rusca – Tihu volcanoclastic formation (RTF) [6]. Red arrows represent the azimuth and sense of the flows and red lines represent only the azimuth of the flows.

3. RESULTS

3.1. ROCK MAGNETISM

To distinguish between soft (magnetite, titanomagnetite) and hard (hematite, goethite) ferromagnetic minerals we have used the S ratio: $S = - \text{IRM}_{-300}/\text{IRM}_{1000}$, where IRM_{1000} is the remanence acquired in a direct field of 1000 mT and IRM_{-300} is the remanence left after applying a backfield of 300 mT. Most of our samples (96.4%) have an S-ratio above 0.90, indicating a ferromagnetic mineralogy dominated by low coercivity magnetic minerals (magnetite and titanomagnetite) [12].

Based on field dependence of magnetic susceptibility we have computed the V index [13]: $V = 100\,(K_{700} - K_{50})/K_{50}$, where K_{50} and K_{700} are magnetic susceptibilities, measured at 50 A/m and at 700 A/m. For our samples, V range between 0.4% and 8.9%, which show the presence of magnetite and titanomagnetite with various content of Ti. Titanomagnetite with higher content of Ti ($V > 2\%$) is present mainly in the

pyroclastic deposits, but not in the sampled lava flows (Fig. 2A). The presence of both magnetite and titanomagnetite is in agreement with thin sections analysis, which shows the presence of lithoclasts of andesite, basalt and, less frequent, diorite.
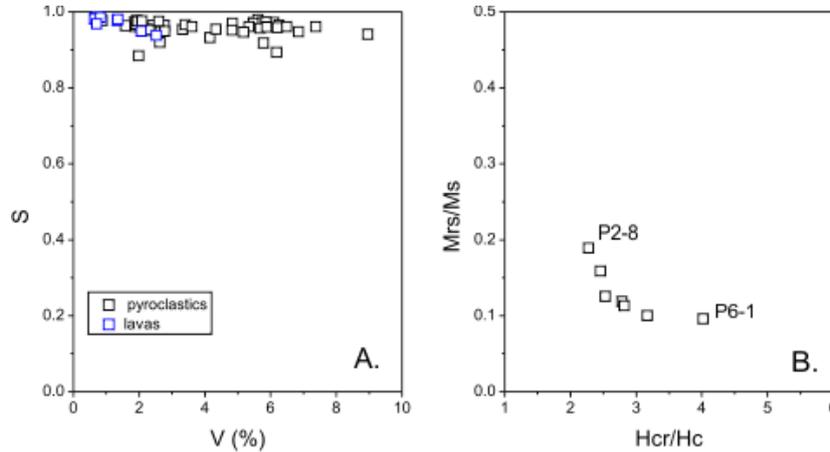

Fig. 2 – A) *S*-ratio *versus V* parameter; B) day-plot of selected samples from pyroclastic deposits. The samples presented in Fig. 3 are marked.
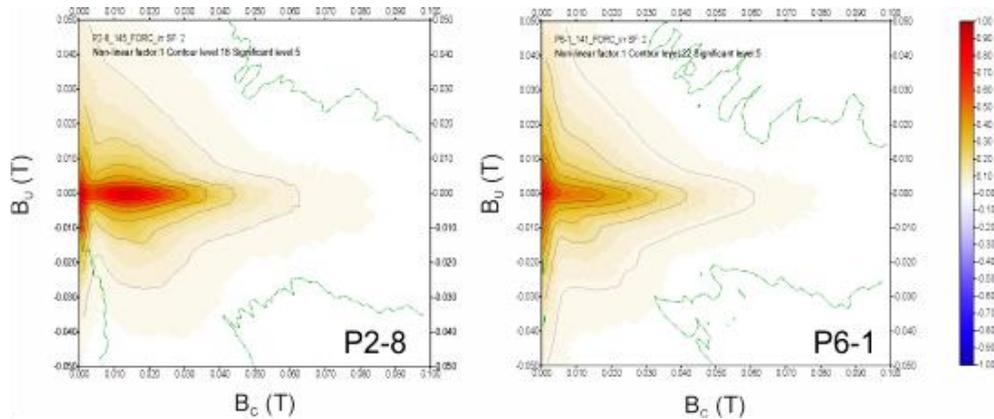

Fig. 3 – FORC diagrams for the samples marked in Fig. 2B.

Based on the hysteresis parameters of selected samples of pyroclasts, we have plotted the Day diagram (Fig 2B), which is widely used to constrain the magnetic domain range of ferromagnetic minerals [14]. The FORC diagram of sample P2-8 (Fig. 3) displays two well defined maxima. The first one is characterized by a central ridge surrounded by closed contours indicating the presence of non-interacting or weakly interacting SD (single domain) particles [*e.g.* 15]. The second one is located at the origin of the FORC diagram with small, '>' shaped open contours. The asymmetry of this second maximum suggests the presence of SP (superparamagnetic)

particles in the sample [15]. The divergence and the triangular shape of outer contours indicate a PSD (pseudo-single domain) background [15]. Sample P6-1 is slightly different (Fig. 3). It displays a single maximum also located near the origin of the FORC diagram, but with contours that are more symmetric around and parallel with Bu axis suggesting an MD (multidomain) contribution rather than an SP one (*e.g.* [15]). The outer contours present the same triangular shape indicating thus a PSD background in this sample as well. The FORC diagrams show that our samples are a mixture of particles with various magnetic domain states. Our results are in agreement with the recent paper of [16], which shows that the Day diagram cannot be alone used to identify the magnetic domain state. However, the data presented in Fig. 2B appear to reveal relative particle size variations in our samples.

Normalized magnetic susceptibility *versus* temperature curves are presented in Fig. 4. The heating curves are in agreement with the values of *S* ratio and *V* parameter. The results show that in samples with *V* larger than 2% there is clear contribution of titanomagnetite with Curie temperature mainly between 300°C and 400°C. Magnetite is dominant in all samples as can be observed from the drop of the curves around 580°C.
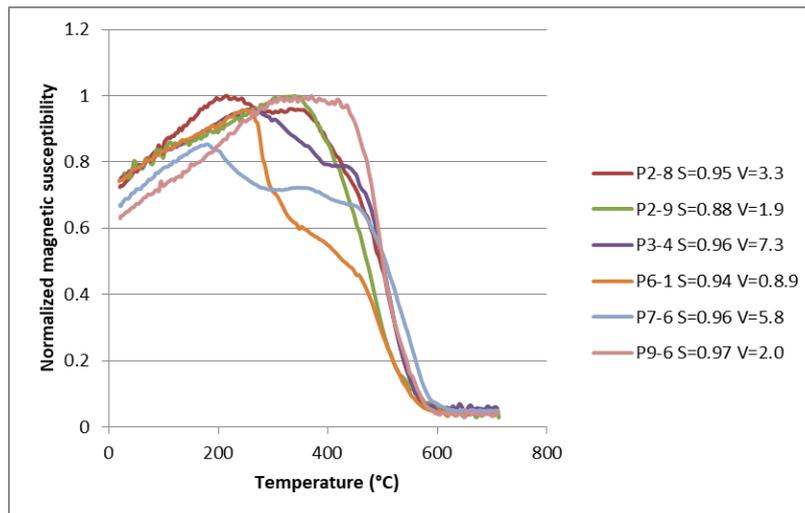

Fig. 4 – Normalized magnetic susceptibility *versus* temperature (heating curves).
For each sample the *S*-ratio and the *V* index are shown.

3.2. PALEOMAGNETIC RESULTS

To gain information about the temperature emplacement of the phreatomagmatic deposit, we analyzed the structure of the natural remanent magnetization of samples from these deposits. The samples were progressively demagnetized using both thermal demagnetization (10–12 steps between room temperature and 600°C) and AF

demagnetization (10 steps up to 100 mT). Typical examples of orthogonal projections are presented in Fig. 5. All analyzed samples had a messy answer both at thermal demagnetization and AF demagnetization and a characteristic remanent magnetization was impossible to identify. This behavior is probably a consequence of the chaotic remanence directions within pyroclastic deposit.
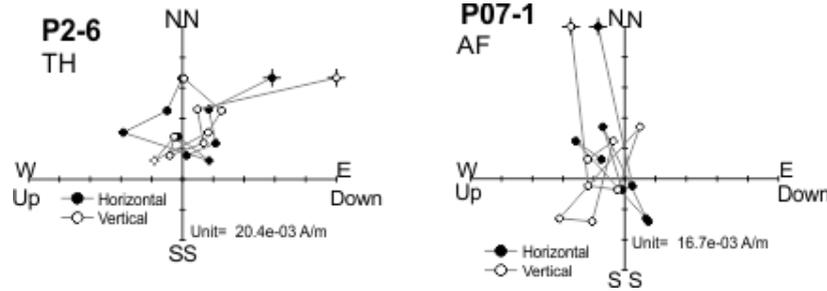

Fig. 5 – Typical orthogonal projection for pyroclastic samples: TH = thermal demagnetization up to 600°C, AF = alternating field demagnetization up to 100 mT.

3.3. ANISOTROPY OF MAGNETIC SUSCEPTIBILITY

In order to evaluate the relationship between depositional processes and magnetic fabrics in the rock record, several parameters were computed to characterize the AMS ellipsoid [17]. The results are presented in Table 1. The statistical treatment of AMS data was done using the Jelinek statistics [17].

Table 1

List of mean anisotropy factors computed at each site: N, number of specimens;
$K_m = (k_{max} + k_{int} + k_{min}) / 3$ (bulk susceptibility); k_{max}, k_{int}, k_{min} (maximum, intermediate, minimum susceptibility); $P' = \exp \{2[(\eta_1 - \eta)^2 + (\eta_2 - \eta)^2 + (\eta_3 - \eta)^2]\}^{1/2}$ (corrected anisotropy degree); $T = 2(\eta_2 - \eta_3) / (\eta_1 - \eta_3) - 1$ (shape parameter); $\eta_1 = \ln k_{max}$, $\eta_2 = \ln k_{int}$, $\eta_3 = \ln k_{min}$, $\eta = (\eta_1 + \eta_2 + \eta_3) / 3$. D, azimuth; I, inclination; E_{1-2}, E_{2-3}, semiangles of the 95% confidence ellipses around the principal magnetic susceptibility axes k_{max} and k_{int}.
Data interpreted as flow directions are in bold

Site	Altitude (m)	N	K_m (10^{-2} SI)	P'	T	$D°, I°$ (k_{max})	$D°, I°$ (k_{min})	$E_{1-2}°$	$E_{2-3}°$
Pyroclastic flows									
P1	772	7	1.12	1.011	0.857	35,3	**149,82**	52	7
P2	656	7	1.17	1.014	0.683	63,1	**161,84**	14	5
P3	658	11	0.98	1.006	0.624	31,9	**247,77**	30	11
P6	773	13	0.97	1.004	0.51	235,5	0,80	29	29
P7	879	7	0.89	1.008	0.787	**154,1**	278,86	19	11
P9	704	6	0.94	1.006	0.042	**154,5**	264,75	25	35
Lava flows									
P8	804	5	2.09	1.018	−0.096	**3,8**	259,59	4	4
C35	828	7	2.00	1.009	0.195	**218,16**	313,16	15	6

The mean magnetic susceptibility K_m of pyroclastites ranges from 0.89×10^{-2} to 1.17×10^{-2} SI, but the interbedded lava flows have a mean susceptibility around 2×10^{-2} SI. The mean corrected anisotropy degree is relative low, which is not unusual for pyroclastic rocks.

The parameter T characterizes the shape of the AMS ellipsoid. If $0 < T < 1$ then the ellipsoid is oblate, which means that the magnetic fabric is planar; if $-1 < T < 0$ then the ellipsoid is prolate, which means that the magnetic fabric is linear; for values of $T = \pm1$ the ellipsoid is uni-axial, while for values of $T \approx 0$ the ellipsoid is tri-axial. Pyroclastic deposits show mostly oblate AMS ellipsoids, while lava flows contain tri-axial AMS ellipsoids, with T around 0 (Fig. 6).
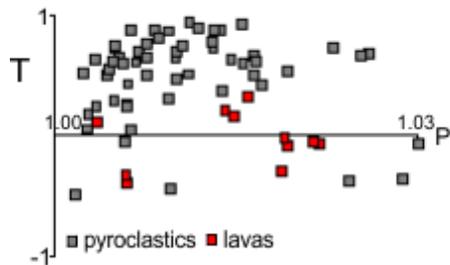

Fig. 6 – Corrected anisotropy degree (P') *versus* shape parameter (T) diagram for all samples.

Magnetic fabric (directions of the principal axes of the AMS ellipsoid) associated with the Rusca-Tihu Formation samples of pyroclastics and lavas are presented in Fig. 7 and 8. In three sites sampled in pyroclastic rocks (P1, P2 and P3, Fig. 7) k_{min} axes are better grouped than either the intermediate and maximum susceptibility axes. The foliation planes are well defined and k_{min} axes are slightly inclined from vertical. The other sites in these rocks (P7, P9 and P6, Fig.7) have vertical k_{min} axes, but the foliation plane is well defined only in site P7. The two sites sampled in lavas have tight distributions for all axes (Fig. 8). Samples yield horizontal k_{max} axes with a N-S orientation (P8) or k_{max} axes are inclined slightly toward the southwest (C35).

4. DISCUSSIONS

For the pyroclastic deposits, we have considered the magnetic foliation as a better indicator of flow direction when it is well defined [18, 19]. Sites P1, P2 and P3 are in this category and we have identified both the azimuth and the sense of the flow (Fig. 7 and Table 1). When the subhorizontal magnetic foliations did not provide useful information for interpreting flow direction, we have used magnetic lineation (sites P7, P9). Since the direction of k_{max} is subhorizontal only the azimuth of the flow can be determined for site P7. For site P9, the azimuth is less reliable

due to high 95% confidence ellipse (Table 1). Site P6 has too dispersed k_{max} and k_{min} axis to define a flow direction. The fast change of the flow direction observed in site P3 with respect to that from the nearby site P2 (Fig. 1) is not unusual in pyroclastic deposits [19].
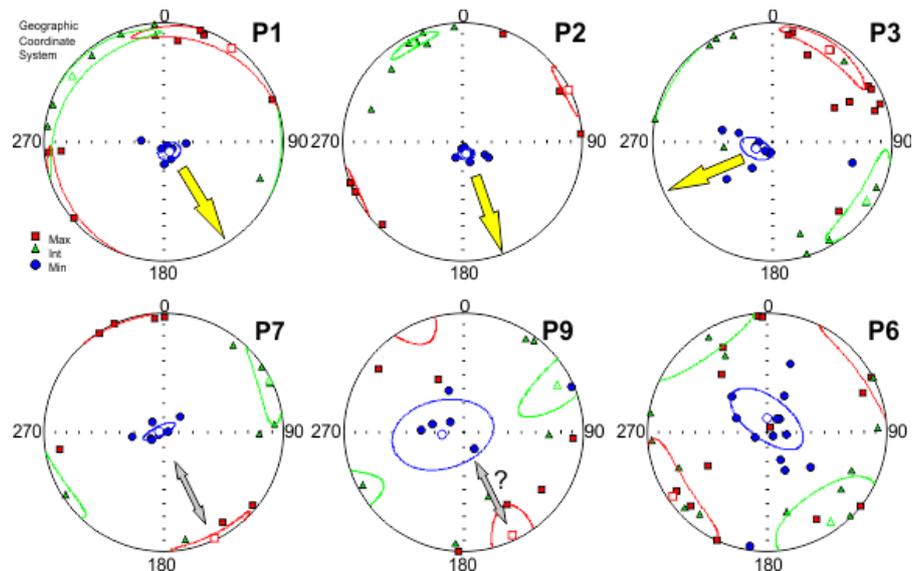

Fig. 7 – Lower hemisphere equal area projections of principal directions of AMS ellipsoids for sites sampled in pyroclastic deposits: red square = maximum magnetic susceptibility k_{max}; green triangle = intermediate magnetic susceptibility k_{int}; blue circle = minimum magnetic susceptibility k_{min}. Directions of mean AMS ellipsoid are represented with open symbols together with their 95% confidence ellipses. The yellow arrow gives the expected azimuth and sense of flow from magnetic foliation. Double head grey arrow shows the expected azimuth of flow from magnetic lineation (Color online).
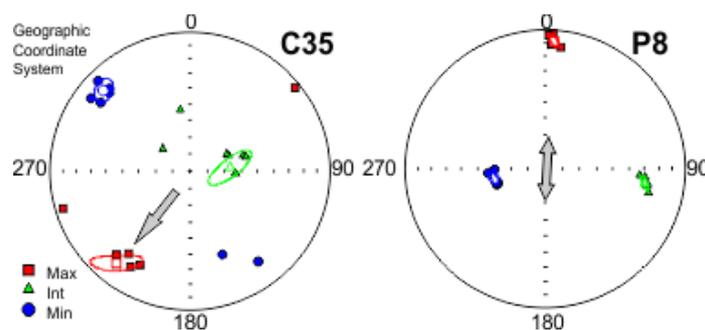

Fig. 8 – Lower hemisphere equal area projections of principal directions of AMS ellipsoids for sites sampled in lava flows. The grey arrow gives the expected azimuth and sense of flow from magnetic lineation. Double head arrow shows the expected azimuth of flow from magnetic lineation. Other symbols are as in Fig. 7 (Color online).

Taking into account both the absence of characteristic remanent magnetizations (Fig. 5) and the Curie temperatures spectrum (Fig. 6), we think that the emplacement temperature of these phreatomagmatic deposits was probably below 300°C. Such low-temperature emplacement of the phreatomagmatic deposits were reported by [20] in Italy.

The most appropriate way to determine the flow direction of lavas is from the k_{max} axis [21]. The azimuth and sense of the lava flow toward southwest was identified for site C35 (Fig. 8). For site P8 it was possible to find only the azimuth of the lava flow, because k_{max} axes are subhorizontal. The azimuths of the lava flows are similar to the azimuth of the pyroclastic flow from the nearby site P7 (Fig. 1).

5. CONCLUSIONS

This AMS and rockmagnetic study reveals several interesting features about the Upper Miocene pyroclastic deposits of the Rusca – Tihu formation from the Călimani Mountains. Both large and small-scale variations in pyroclastic and lava flow directions are observed in the AMS results, which show that the transportation and depositional mechanisms changed with time [20]. Overall, the general trend of flow directions toward south is compatible with the supposed position of the eruption centers (Fig. 1). The emplacement temperature of the studied pyroclastic deposits was probably below 300°C.

This pioneer work shows that the AMS method, if it will be systematically applied to the ancient large-volume pyroclastic deposits from the Călimani Mountains, can provide information about the location of the source vents and transportation and depositional mechanisms.

REFERENCES

1. M.H. Ort, M. Porreca and J.W. Geissman, Geological Society, London, Special Publications **396**, 1–11 (2015).
2. F. Hrouda, Geophysical Surveys **5**(1), 37–82 (1982).
3. N. Lenhardt, H. Böhnel, M. Hinderer and J. Hornung, Sedimentary Geology **290**, 1–14 (2013).
4. C. Panaiotu, C. Necula, T. Merezeanu, A. Panaiotu and C. Corban, Romanian Reports in Physics **63**(2), 526–534 (2011).
5. I. Seghedi, H. Downes, A. Szakács, P.R.D. Mason, M.F. Thirlwall, E. Roşu, Z. Pécskay, E. Márton and C.G. Panaiotu, Lithos **72**(3–4), 117–146 (2004).
6. I. Seghedi, A. Szakács, Z. Pécskay and P.R.D. Mason, Geologica Carpathica **56**(1), 67–75 (2005).
7. A. Szakács and I. Seghedi, Romanian Journal of Petrology **77**(1), 1–55 (1996).

8. A. Szakács and I. Seghedi, *Large volume volcanic debris avalanche in the East Carpathians, Romania.* Gordon Breach Science Publishers, the Netherlands, 131–151 (2000).

9. A. Țugui, C. Necula, C. Panaiotu, Romanian Reports in Physics **61**(3), 730–739 (2009).

10. X. Zhao, D. Heslop, and A. P. Roberts, Geochem. Geophys. Geosyst. **16**, 1364–1377 (2015).

11. C.G Panaiotu, D. Dimofte, C. Necula, A. Dumitru, I. Seghedi, R.-G. Popa, Romanian Reports in Physics **68**, 1, 416–424 (2016).

12. M.E. Evans, F. Heller, *Environmental Magnetism: Principles and Applications of Environmagnetics*, Academic Press Elsevier Science, Amsterdam, 2003.

13. F. Hrouda, M. Chlupáčová and Š.Mrázová, Physics of the Earth and Planetary Interiors **154**(3–4), 323–336 (2006).

14. D.J Dunlop, J. Geophys. Res. **107** (B3), 2056 (2002).

15. A. P Roberts, D. Heslop, X. Zhao and C. R. Pike,. Reviews of Geophysics **52**(4), 557–602 (2014).

16. A. P. Roberts, L. Tauxe, D. Heslop, X. Zhao and Z. Jiang, Journal of Geophysical Research: Solid Earth **123** (2018).

17. D.H. Tarling and F. Hrouda, *The magnetic anisotropy of rocks*, Chapman and Hall, London, 1993.

18. Porreca, M., M. Mattei, G. Giordano, D. De Rita, and R. Funiciello, Magnetic fabric and implications for pyroclastic flow and lahar emplacement, Albano maar, Italy, J. Geophys. Res., 108(B5), 2264, (2003).

19. R. D. LaBerge, M. Porreca, M. Mattei, G. Giordano and R. A.F. Cas, Tectonophysics **466**, 64–78 (2009).

20. E. Cañón-Tapia, Geological Society, London, Special publications **238**, 205–225 (2004).